RadioGraphics

Multimodality Imaging of Neoplastic and Nonneoplastic Solid Lesions of the Pancreas[1]

Gavin Low, MBChB, MRCS, FRCR • Anukul Panu, MD • Noam Millo, MD • Edward Leen, MD, FRCR

CME FEATURE

See www.rsna.org/education/rg_cme.html

LEARNING OBJECTIVES FOR TEST 5

After completing this journal-based CME activity, participants will be able to:

- Identify the imaging features of various solid pancreatic lesions.
- Discuss clinical information that can aid in the diagnosis of neoplastic and nonneoplastic solid lesions of the pancreas.
- Describe clinical and imaging features that can help distinguish pancreatic adenocarcinoma from other pancreatic lesions.

TEACHING POINTS

See last page

Solid lesions of the pancreas represent a heterogeneous group of entities that can be broadly classified as either neoplastic or nonneoplastic. Neoplastic lesions include pancreatic adenocarcinoma, pancreatic neuroendocrine tumor, solid pseudopapillary tumor, pancreatoblastoma, pancreatic lymphoma, metastases to the pancreas, and rare miscellaneous neoplasms. Nonneoplastic lesions include focal pancreatitis, fatty infiltration-replacement, intrapancreatic accessory spleen, congenital anomalies such as prominent pancreatic lobulation and bifid pancreatic tail (pancreatic bifidum), and rare miscellaneous lesions (eg, pancreatic sarcoidosis, Castleman disease of the pancreas). A variety of imaging modalities are available for assessing these solid lesions, including ultrasonography (US), computed tomography (CT), magnetic resonance imaging, endoscopic US, and hybrid nuclear imaging techniques such as single photon emission computed tomography–CT and positron emission tomography–CT, each of which has its own strengths and limitations. Accurate diagnosis can be challenging, and use of a multimodality imaging approach is often helpful in equivocal or complex cases. Knowledge of relevant clinical information and key radiologic features is essential for confident lesion characterization and differentiation.

Abbreviations: AIP = autoimmune pancreatitis, CBD = common bile duct, FDG = 2-[fluorine-18]fluoro-2-deoxy-D-glucose, HDRBC = heat-damaged red blood cell, IPAS = intrapancreatic accessory spleen, MPD = main pancreatic duct, NET = neuroendocrine tumor, RCC = renal cell carcinoma, SPT = solid pseudopapillary tumor

RadioGraphics 2011; 31:993–1015 • **Published online** 10.1148/rg.314105731 • **Content Codes:** GI OI

[1]From the Department of Radiology and Diagnostic Imaging, University of Alberta Hospital, 2A2.41 Walter Mackenzie Center, 8440-112 St, Edmonton, AB, Canada T6G 2B7 (G.L., A.P., N.M.); and Department of Imaging Science, Imperial College London, Hammersmith Hospital, London, England (E.L.). Received June 23, 2010; revision requested July 30 and received August 12; accepted August 20. For this journal-based CME activity, the authors (G.L., A.P., N.M.), editor, and reviewers have no relevant relationships to disclose. E.L. received research grants from Bracco and AngioDynamics and equipment support from Koninklijke Philips Electronics, GE Healthcare, and SuperSonic Imagine. **Address correspondence to** G.L. (e-mail: *timgy@yahoo.com*).

Introduction

Solid lesions of the pancreas, broadly classified as neoplastic and nonneoplastic lesions, are increasingly encountered in the course of routine radiology practice due to escalating imaging volumes and greater diagnostic capabilities of contemporary imaging techniques. Solid pancreatic lesions may be detected at imaging as an expected finding in patients who undergo work-up for clinically suspected pancreatic disease. However, a significant number of these lesions are discovered incidentally at imaging performed for an unrelated clinical indication (1). Accurate and timely imaging diagnosis is essential because it facilitates patient triage, guides clinical management, and helps determine patient prognosis. Some lesions require surgery or follow-up imaging, whereas others are clinically insignificant and require no further action. Technologic advances in imaging, such as multisection computed tomography (CT), magnetic resonance (MR) imaging, endoscopic ultrasonography (US), and hybrid nuclear imaging techniques (eg, single photon emission computed tomography [SPECT]/CT and positron emission tomography [PET]/CT), allow solid pancreatic lesions to be characterized on the basis of morphologic, hemodynamic, and metabolic findings. Use of a multimodality approach combines the strengths of individual imaging modalities and has a synergistic effect in improving diagnostic yield. Such an approach is especially helpful in equivocal or complex cases.

In this article, we review solid lesions of the pancreas in terms of relevant clinical information and key radiologic features that allow confident lesion characterization and differentiation from other disease entities.

Neoplastic Solid Lesions

Pancreatic Adenocarcinoma

Pancreatic adenocarcinoma accounts for 85%–95% of all pancreatic malignancies and is the fourth leading cause of cancer-related deaths (2). Most patients are 60–80 years of age, and males are affected twice as often as females (2). Of these tumors, 60%–70% are located in the pancreatic head, 10%–20% in the body, and 5%–10% in the tail. Diffuse glandular involvement occurs in 5% of cases. Abdominal pain, weight loss, and jaundice are the main presenting complaints but generally occur late in the disease course. Prognosis is poor, with a 1-year survival rate of less than 20% and a 5-year survival rate of less than 5% (3). Nonresectable disease is seen at presentation in 75% of patients, with metastases (mainly to the liver and peritoneum) present in 85% of these patients (2). Surgery is the only cure, with a postoperative 5-year survival

Table 1
NCCN Practice Guidelines in Oncology: Criteria for Defining the Resectability Status of Pancreatic Adenocarcinoma

Resectable
No distant metastases
No SMV or PV abutment, distortion, tumor thrombus, or venous encasement
Clear fat planes around the CA, SMA, and HA
Borderline resectable
No distant metastases
Venous involvement of the SMV or PV consisting of tumor abutment with or without impingement and narrowing of the vessel lumen
Encasement of the SMV or PV but without encasement of the nearby arteries
Short-segment venous occlusion resulting from either tumor thrombus or encasement but with suitable vessel proximal and distal to the area of tumor involvement, allowing safe resection and reconstruction
Gastroduodenal artery encasement up to the HA with either short-segment encasement or direct abutment of the HA, without extension to the CA
Tumor abutment of the SMA ≤ 180° of the circumference of the vessel wall
Unresectable
Pancreatic head
Distant metastases
SMA encasement >180°, any CA abutment
Unreconstructible occlusion of the SMV or PV
Aortic invasion or encasement
Pancreatic body
Distant metastases
SMA or CA encasement >180°
Unreconstructible occlusion of the SMV or PV
Aortic invasion
Pancreatic tail
Distant metastases
SMA or CA encasement >180°
Nodal status
Metastases to lymph nodes beyond the field of resection

Source.—Reference 4.
Note.—CA = celiac axis, HA = hepatic artery, NCCN = National Comprehensive Cancer Network, PV = portal vein, SMA = superior mesenteric artery, SMV = superior mesenteric vein.

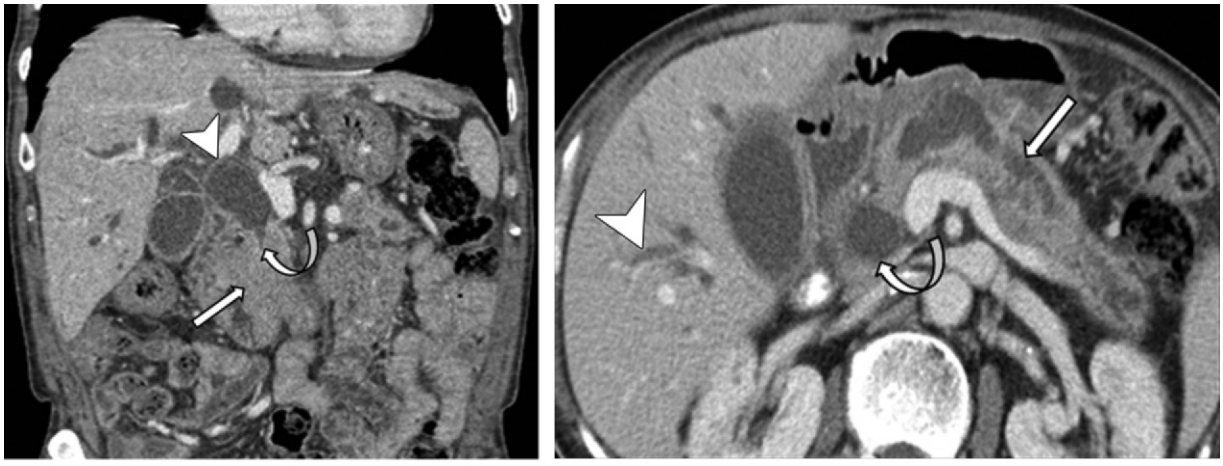

a. b.

Figure 1. Adenocarcinoma in a 78-year-old man with a 3-week history of increasing weakness, abdominal pain, and jaundice. **(a)** Coronal postcontrast portal phase CT scan shows an isoattenuating tumor (straight arrow) in the pancreatic head causing proximal dilatation (arrowhead) and abrupt distal narrowing (curved arrow) of the common bile duct (CBD). **(b)** Axial postcontrast portal phase CT scan shows the double duct sign—simultaneous dilatation of the MPD (straight arrow) and CBD (curved arrow)—due to an obstructing mass. Intrahepatic ductal dilatation (arrowhead) is also present.

Figure 2. Unresectable adenocarcinoma with vascular invasion and liver metastases in a 72-year-old man with abdominal pain, weight loss, and jaundice. Postcontrast portal phase CT scan shows encasement of the celiac axis and occlusion of the portal vein by a diffuse, hypoattenuating pancreatic tumor (curved arrow). Multiple ill-defined hypoattenuating liver metastases (straight arrow) are also present.

rate of 20% (2). Accurate detection and staging are essential for ensuring appropriate selection of patients who will benefit from surgery and for preventing unnecessary surgeries in patients with unresectable disease. The criteria for defining the resectability status of pancreatic adenocarcinoma are shown in Table 1 (4).

Teaching Point

High-resolution dual-phase (arterial and portal) contrast material–enhanced CT is the established technique for evaluating pancreatic adenocarcinoma. Arterial phase imaging (performed 20–40 seconds after contrast agent injection) allows optimal visualization of the tumor and peripancreatic arteries. Maximal contrast between the hypovascular tumor and the normal pancreas yields optimal tumor conspicuity in this phase. Most tumors are hypoattenuating, with a mean size of 3 cm (range, 1.5–10 cm; average size in the pancreatic head, 2.5–3 cm; average size in the body and tail, 5–7 cm) (2). Portal phase imaging (performed 50–70 seconds after injection) is optimal for detecting metastatic disease to the liver and for assessing the peripancreatic veins.

No pancreatic mass is visualized in 10% of cases, since the tumor may be isoattenuating (Fig 1a) (3). The presence and location of a mass may be inferred from secondary signs such as mass effect, an abnormal convex contour of the pancreas, ductal obstruction, and vascular invasion (2,3). Tumors in the pancreatic head may cause dilatation of both the CBD and the main pancreatic duct (MPD), known as the "double duct sign" (Fig 1b), whereas tumors in the pancreatic body may cause upstream MPD dilatation. Atrophy of the pancreas proximal to the tumor is noted in chronic obstruction. A circumferential soft-tissue cuff around the peripancreatic vessels with loss of the perivascular fat plane denotes vascular invasion (Fig 2). A sensitivity of 84% and a specificity of 98% for invasion are reported if the tumor is contiguous with more than 50% of the vessel circumference (5). Other features suggesting vascular invasion include vessel deformity, thrombosis,

and development of collateral vessels. The "teardrop sign" refers to an alteration of the superior mesenteric vein from its normal round shape to a teardrop shape on axial images secondary to tumor infiltration or peritumoral fibrosis (6). Cystic-necrotic degeneration, an uncommon feature of adenocarcinoma, is present in 8% of cases (Fig 3) (7). Metastases are most commonly found in the liver (Fig 2) and peritoneum (Fig 4). CT has an accuracy of 85%–95% for tumor detection, a positive predictive value of 89%–100% for unresectability, and a negative predictive value of 45%–79% for resectability (3).

Adenocarcinoma has low signal intensity on T1- and T2-weighted MR images secondary to its scirrhous fibrotic nature. As at CT, the hypovascular tumor enhances less than the normal pancreas at MR imaging, although a thin peritumoral rim of greater enhancement is often observed, which may help establish disease focality. MR imaging has better contrast resolution than CT and is superior in detecting small tumors and metastases. The accuracy of MR imaging in the detection and staging of adenocarcinoma is 90%–100% (8).

Endoscopic US, a high-resolution imaging method, has a recognized role in the detection and staging of small tumors. It can help detect masses as small as 0.2–0.3 cm. Endoscopic US can clarify equivocal findings at CT or MR imaging and allows biopsy of suspect lesions. Adenocarcinoma appears as an ill-defined, heterogeneous hypoechoic mass at endoscopic US (Fig 5). DeWitt et al (9) found endoscopic US to be more sensitive than CT in detecting adenocarcinoma (98% versus 86%) and more accurate in tumor staging (67% versus 47%). However, endoscopic US does have certain limitations. It is highly operator dependent, with a relatively steep learning curve. It is also characterized by a narrow field of view, so that it is limited in the assessment of locoregional invasion or involvement of vessels other than the portal vein.

PET is an emerging technique for characterizing tissue on the basis of functional rather than morphologic information. The principle of 2-[fluorine-18]fluoro-2-deoxy-D-glucose (FDG) PET is that malignant tissues have greater uptake and retention of FDG than does normal tissue due to enhanced glucose metabolism. Pancreatic adenocarcinoma generally shows intense focal FDG uptake (Fig 6). In a study of 74 patients with a pancreatic mass, Inokuma et al (10) prospectively compared the performance of FDG PET with that of CT, transabdominal US, and endoscopic US in the diagnosis of adenocarcinoma. They found that the sensitivity and specificity of FDG PET (96% and 78%, respectively) were superior to those of CT (91% and 56%), transabdominal US (91% and 50%), and endoscopic US (96%

Figure 3. Adenocarcinoma with extensive cystic-necrotic degeneration in a 58-year-old man with progressive weight loss and jaundice. Postcontrast arterial phase CT scan shows a large exophytic tumor in the pancreatic head with solid (straight arrow) and cystic-necrotic (curved arrow) components.

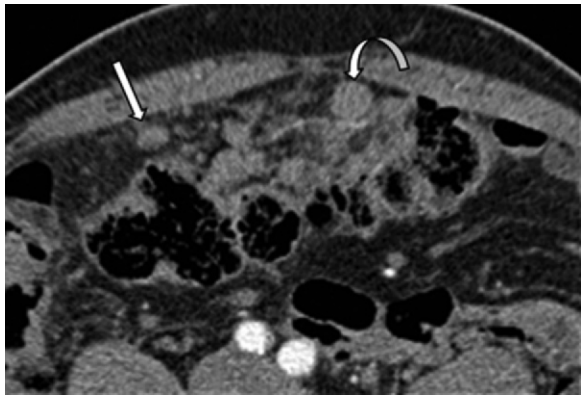

Figure 4. Peritoneal metastases in the same patient as in Figure 3. Postcontrast arterial phase CT scan shows multiple round (curved arrow) and ovoid (straight arrow) peritoneal metastases.

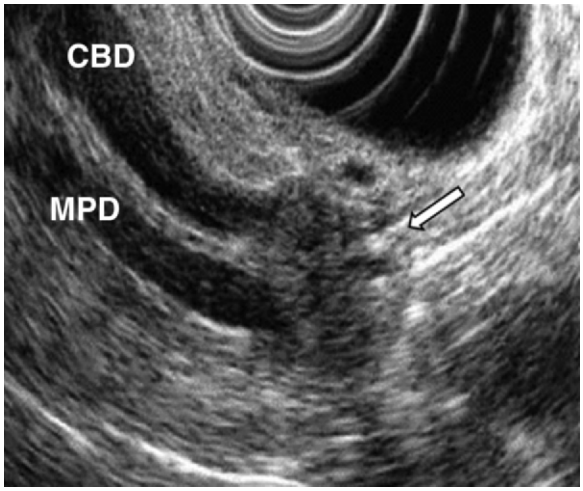

Figure 5. Adenocarcinoma with the double duct sign. Endoscopic US image shows an ill-defined, heterogeneous hypoechoic tumor (arrow) in the pancreatic head causing obstruction of the MPD and CBD. (Courtesy of Gurpal Sandha, MD, University of Alberta Hospital, Edmonton, Alberta, Canada.)

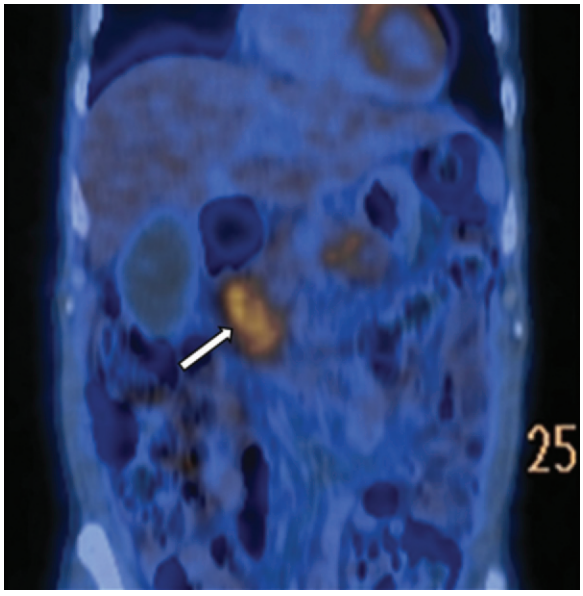

Figure 6. Adenocarcinoma in a 78-year-old man (same patient as in Figure 1). Coronal fused FDG PET/CT image shows the tumor with hypermetabolic focal FDG uptake (arrow).

and 67%). In an analysis of six studies, Berberat et al (11) found that PET had an accuracy of 85%–93%, a sensitivity of 85%–100%, and a specificity of 84%–93% in the detection of adenocarcinoma. The biggest potential impact of FDG PET is in the detection of small metastases, an area in which CT (45%–79% negative predictive value for resectability) and MR imaging generally underperform. Frohlich et al (12) found that FDG PET helped detect 97% of liver metastases larger than 1 cm and 43% of metastases smaller than 1 cm, with a specificity of 95%. The recent development of hybrid scanners for PET/CT, a combined physiologic-anatomic modality, will enhance the diagnostic capabilities of PET in the characterization of pancreatic masses.

False-positive and false-negative cases represent limitations of FDG PET. Tumor detection at FDG PET depends on both tumor size and the degree of tumor-to-background FDG uptake. Underestimation of uptake may occur in small tumors due to partial volume averaging and in tumors that are located adjacent to areas of physiologic uptake. Ampullary tumors are an example of this phenomenon, due to their small size at the time of clinical presentation and their proximity to FDG-avid bowel. False-negative cases may occur in mucinous tumors (reduced uptake due to tissue hypocellularity); necrotic tumors containing minimal viable tissue; peritoneal metastases smaller than 1 cm; and patients with hyperglycemia, in whom there is reduced uptake due to competitive inhibition. False-positive cases may occur in inflammatory tissue due to mild to moderate uptake by inflammatory mediators, fibroblasts, and granulation tissue. This uptake may be seen in pancreatitis following recent radiation therapy, at sites of recent surgical incision and biopsy, and around CBD stents.

Pancreatic Neuroendocrine Tumor

Pancreatic neuroendocrine tumors (NETs), a subset of gastroenteropancreatic NETs according to the World Health Organization classification system, were previously referred to as islet cell tumors because they were thought to have originated from the islets of Langerhans. However, new evidence suggests that these tumors originate from pluripotential stem cells in ductal epithelium (13). They account for 1%–5% of all pancreatic tumors, have equal gender distribution, and typically manifest in patients aged 51–57 years. Most cases are sporadic, but association

with syndromes such as multiple endocrine neoplasia type 1, von Hippel–Lindau syndrome, neurofibromatosis type 1, and tuberous sclerosis has been observed. NETs are classified into functioning and nonfunctioning tumors. Functioning tumors produce symptoms related to excessive hormone production. They account for 15%–52% of all tumors (14) and are subdivided according to the hormones they produce. The features of both functioning and nonfunctioning NETs are presented in Table 2.

A variety of imaging appearances exist. Tumors tend to be multiple, especially when associated with syndromes such as multiple endocrine neoplasia type 1 and von Hippel–Lindau syndrome. Single lesions are seen in 90% of insulinomas, whereas multiple lesions are present in 20%–40% of gastrinomas. Tumor size is variable. In general, functioning tumors manifest early in the course of disease when they are small, due to the clinical manifestations of excessive hormone production. Nonfunctioning tumors manifest when they are large, due to mass effect. Risk of malignancy increases with tumor size (especially in tumors >5 cm), with 90% of nonfunctioning tumors being malignant at presentation (14). Tumor morphologic features are also variable. Small tumors are generally solid and homogeneous, whereas larger tumors are heterogeneous and may show cystic-necrotic degeneration (Fig 7) and calcification (Fig 8) (14). Malignant tumors may show features of local spread, vascular invasion, lymph node involvement, and organ metastases.

NETs share some common distinguishing features. At MR imaging, these tumors generally have longer T1 and T2 relaxation times than do the normal pancreas and most other pancreatic neoplasms. Consequently, relative to the normal pancreas, most NETs have low signal intensity on T1-weighted MR images and intermediate to high signal intensity on T2-weighted images. The most distinctive feature of NETs is their behavior at contrast-enhanced imaging. NETs have a rich vascular supply and therefore enhance avidly during the arterial phase, enhancing more rapidly and intensely than the normal pancreas (Fig 9a, 9b) (14). Homogeneous enhancement is typical

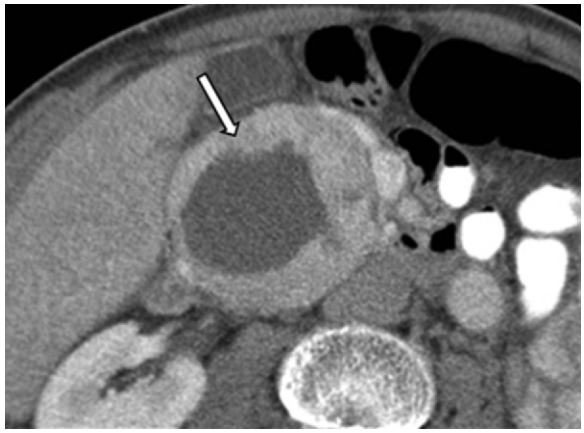

Figure 7. Malignant NET with cystic-necrotic degeneration in a 69-year-old man with obstructive jaundice. Postcontrast portal phase CT scan shows a large tumor (arrow) in the uncinate process with extensive cystic-necrotic degeneration and a thick enhancing wall. (Courtesy of Iain Birchall, MD, University of Alberta Hospital, Edmonton, Alberta, Canada.)

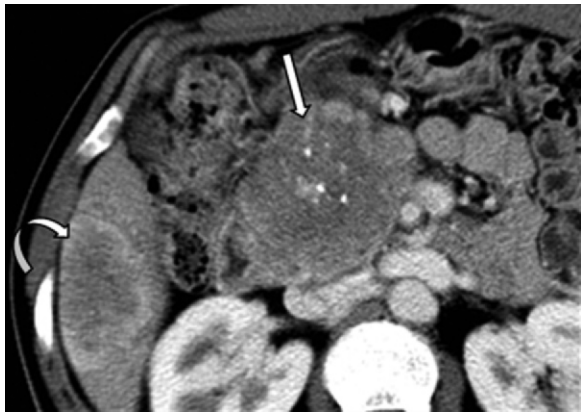

Figure 8. Malignant NET with liver metastases in a 53-year-old man with general malaise. Postcontrast arterial phase CT scan shows a heterogeneous hypoattenuating tumor in the pancreatic head containing punctate foci of calcification (straight arrow). A large, hypervascular ring-enhancing metastasis (curved arrow) is seen in segment VI of the liver.

Teaching Point

Table 2
Features of Pancreatic NETs

Tumor*	Malignancy	Location	Signs and Symptoms	Survival
Functioning tumors (15%–52%)				
Insulinoma (50%) [<2 cm, 90% of cases; <1.5 cm, 66%; <1 cm, 40%]	10% are malignant	90% are in the pancreas, equal glandular distribution	Hypoglycemic attacks, atypical seizures	Generally 100% after resection
Gastrinoma (20%) [mean, 4 cm]	60% are malignant, metastases seen in up to 60%	25%–60% are in the pancreas; 90% occur in the gastrinoma triangle (junction between the bile duct and cystic duct superiorly, pancreatic body medially, and duodenum inferiorly)	Zollinger-Ellison syndrome with peptic ulceration and diarrhea	10-year survival rate of 90% following complete resection
Glucagonoma (1%) [most commonly 2–6 cm]	70% are malignant, metastases seen in up to 60%	>90% are in the pancreas, with a predilection for the body and tail	Necrolytic migratory erythema, weight loss, diabetes, diarrhea	More favorable with complete resection, prolonged even with liver metastases
Vipoma (3%) [mean, 5 cm]	Up to 75% are malignant, metastases seen in up to 70%	90% are in the pancreas (most commonly the tail), 10%–20% are extrapancreatic (most commonly in the retroperitoneal sympathetic chain and adrenal glands)	Werner-Morrison syndrome with watery diarrhea and hypokalemia	5-year survival rate of 95% following complete resection (60% in patients with metastases)
Somatostatinoma (<1%) [often >5 cm]	50% are malignant, metastases seen in up to 50%	50% are in the pancreas and 50% in the duodenum	Gallstones, weight loss, diarrhea, steatorrhea, diabetes	5-year survival rate of 95% following complete resection (60% in patients with metastases)
Nonfunctioning tumors (15%–50%) [>10 cm in 30% of cases; range, 3–24 cm]	90% are malignant, metastases seen in up to 50%	Predilection for the pancreatic head	Abdominal pain and distention, jaundice, weight loss, gastrointestinal bleeding from splenic vein compression†	5-year survival rate >50% following complete resection

*Numbers in parentheses indicate percentage of all pancreatic NETs. Tumor size in brackets.
† Signs and symptoms of nonfunctioning tumors are caused by mass effect.

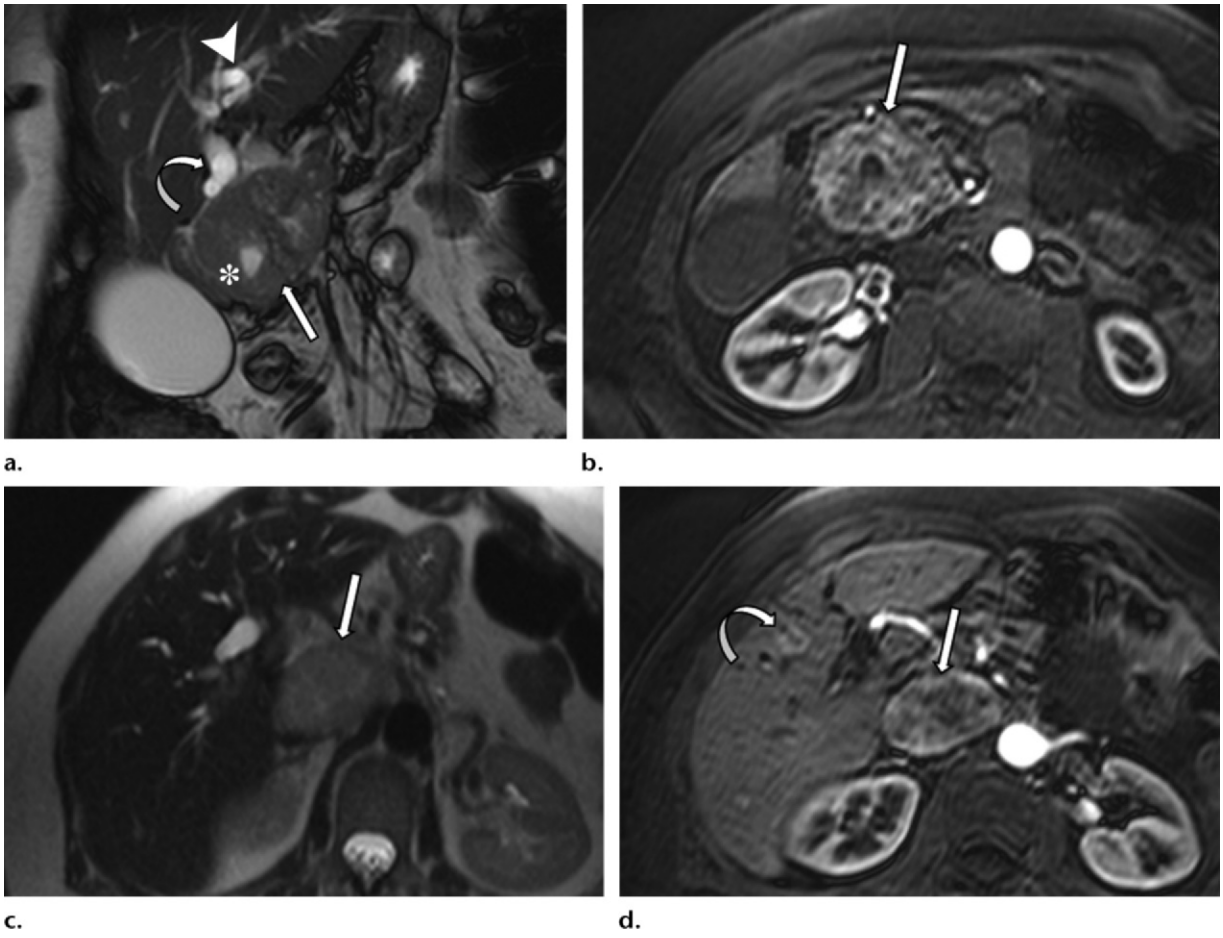

Figure 9. Malignant NET with liver and lymph node metastases in a 66-year-old woman with obstructive jaundice. **(a)** Coronal T2-weighted MR image shows a tumor (straight arrow) in the pancreatic head with internal cystic-necrotic degeneration (*) causing dilatation of the CBD (curved arrow) and intrahepatic duct (arrowhead). **(b)** Axial postcontrast arterial phase T1-weighted MR image shows the tumor with heterogeneous hyperenhancement (arrow). **(c)** Axial T2-weighted MR image shows a heterogeneously hyperintense portocaval lymph node metastasis (arrow). **(d)** Axial postcontrast arterial phase T1-weighted MR image shows heterogeneous enhancement of the portocaval lymph node metastasis (straight arrow) and a small ring-enhancing liver metastasis (curved arrow), which was detected only after contrast material administration. The liver and lymph node metastases demonstrate hyperenhancement similar to that of the primary tumor.

for small tumors less than 2 cm, whereas larger lesions tend to show heterogeneous enhancement, which can be ringlike (14). Capturing this vascular blush is essential for the diagnosis of small tumors such as insulinoma, which often do not distort the contour of the pancreas. During the portal phase, tumors may be either hyper-, iso-, or hypoenhancing relative to the normal pancreas. Some tumors demonstrate atypical delayed enhancement and are best appreciated at portal phase imaging (14). Metastases to lymph nodes and solid organs such as the liver may have an enhancement pattern similar to that of the primary tumor (Fig 9c, 9d). For clinically suspected NET, high-resolution dual-phase CT or MR imaging should be performed for optimal tumor detection, characterization, and staging. Gouya et al (15) found that thin-section biphasic CT, non-thin-section biphasic CT, and sequential CT had sensitivities of 94.4%, 57%, and 28.6%, respectively, in the diagnosis of insulinoma. MR imaging has a sensitivity of 85%–94% (16,17).

Endoscopic US and indium 111 (^{111}In) octreotide SPECT/CT play a role in the evaluation of

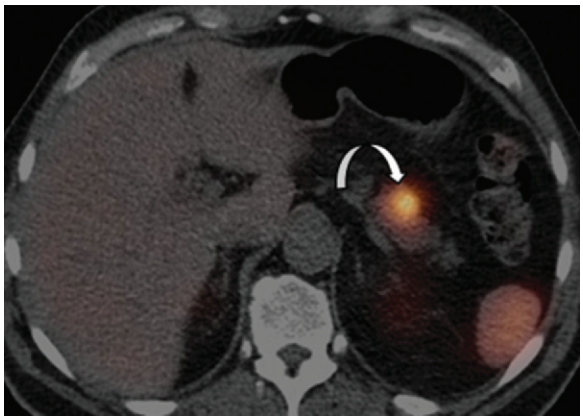

Figure 10. NET in a 69-year-old man with presyncopal episodes and atypical chest discomfort. Axial fused ^{111}In octreotide SPECT/CT image shows a small tumor of the pancreatic body and tail with high focal uptake (arrow). Physiologic low-grade uptake is seen in the liver and spleen.

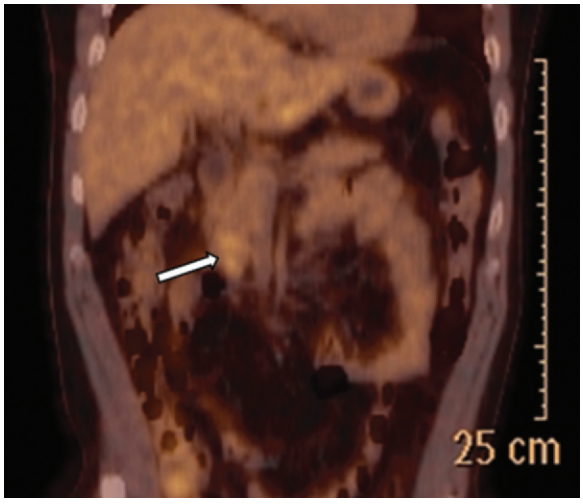

Figure 11. Malignant NET in a 42-year-old man with multiple endocrine neoplasia type 1 syndrome. Coronal fused FDG PET/CT image shows a tumor of the uncinate process with hypermetabolic focal uptake (arrow). Physiologic uptake is demonstrated elsewhere in the image. A diagnosis of pancreatic NET was confirmed at contrast-enhanced CT.

NETs. In the study by Gouya et al (15), the sensitivity of endoscopic US for diagnosing insulinoma was 93.8%, and the sensitivity of combined thin-section dual-phase CT and endoscopic US was 100%. ^{111}In-radiolabeled octreotide (somatostatin analog) is taken up by somatostatin receptors 2 and 5, which are found in most NETs but not in insulinoma (Fig 10). The sensitivity and specificity of ^{111}In octreotide imaging for detecting functional pancreatic NETs (except insulinoma) are 90% and 80%, respectively (18). Insulinomas rarely express somatostatin receptors, thus limiting the sensitivity of ^{111}In octreotide imaging in their detection to 10%–50% (18). The use of SPECT/CT improves image interpretation by providing better attenuation correction, increased specificity, more accurate localization of disease, and clarification of adjacent organ involvement. In practice, the main advantage of octreotide imaging is that it allows whole-body scanning for the detection of small tumors and metastases, including in areas that are not under clinical suspicion. FDG PET may have a role in the assessment of poorly differentiated NETs, which are generally octreotide negative. These tumors exhibit increased uptake at FDG PET (Fig 11) because they have a high proliferative rate, unlike well-differentiated tumors, which show poor uptake due to low proliferative rates.

It is important to differentiate NETs from other tumors of the pancreas, particularly adenocarcinoma, since the prognoses (NET patients have a better prognosis) and treatment options differ. Several criteria can aid in differentiating NET from adenocarcinoma (14).

1. Enhancement. Adenocarcinoma is a hypovascular tumor, whereas NET is generally hypervascular.

2. Calcification. Only 2% of adenocarcinomas show calcification, compared with 20% of NETs.

3. Vascular involvement. Adenocarcinomas are associated with vascular encasement, whereas malignant NETs may show vascular infiltration with tumor thrombus.

4. Ductal involvement. Adenocarcinoma has a high propensity for ductal obstruction, but this finding is uncommon in NET.

5. Central necrosis and cystic degeneration. These findings are more common in NETs than in adenocarcinomas.

Solid Pseudopapillary Tumor

First described in 1959 by Franz (19), solid pseudopapillary tumor (SPT) has been called by many different names, including *solid cystic papillary epithelial tumor*, *papillary cystic tumor*, and *solid and cystic tumor*. In 1996, the World

Health Organization renamed it *solid pseudopapillary tumor* (20). SPT accounts for 1%–2% of all pancreatic tumors. It is most common in females (9:1 female predilection), young adults (mean age, 25 years; range, 10–74 years) (21), and African and Asian individuals. SPT has a low malignant potential with an excellent prognosis following complete resection. Metastases are uncommon, occurring in 7%–9% of cases, mostly to the liver, omentum, and peritoneum (22). The most common presenting complaints are pain and an abdominal mass, although SPT may be asymptomatic in up to 15% of cases.

SPT is typically a large (mean, 9 cm), slow-growing, well-encapsulated mass (21,23). It most commonly occurs in the pancreatic tail, followed closely by the pancreatic head. SPT has a tendency to displace rather than invade surrounding structures and rarely causes obstruction of the bile duct or pancreatic duct. The pseudocapsule (composed of compressed pancreatic tissue and reactive fibrosis) has low attenuation at CT and low signal intensity at T1- and T2-weighted MR imaging. Internal hemorrhagic and cystic degeneration is the hallmark of SPT due to the fragile vascular network of the tumor. These imaging features are best appreciated at MR imaging (Fig 12). Subacute hemorrhage may appear hyperintense on T1-weighted images and have variable signal intensity on T2-weighted images, whereas chronic hemorrhage is hypointense with both sequences. A fluid-fluid or fluid-debris level is detected in 10%–18% of cases due to the hematocrit effect (21). Peripheral calcification is present in 30% of cases (21). Typically, SPT shows peripheral heterogeneous enhancement during the arterial phase and progressive nonuniform enhancement thereafter, with enhancement generally being less than that of the normal pancreas (24). The main differential consideration is cystic NET. There are several features that can help distinguish between SPT and cystic NET.

Teaching Point

1. Age at presentation. NETs rarely occur in patients younger than 30 years of age.

2. Signal intensity at T1-weighted MR imaging. NET has low signal intensity; SPT, which contains hemorrhage, may have high signal intensity.

3. Tumor enhancement characteristics. NETs are more vascular and demonstrate either diffuse or ringlike hyperenhancement.

Pancreatoblastoma

Pancreatoblastoma accounts for 0.2% of all pancreatic tumors and is the most common pancreatic tumor in young children (25). At histologic analysis, it resembles the incompletely differentiated acini of fetal pancreatic tissue at 7 weeks gestational age (25,26). Two categories of pancreatoblastoma have been reported on the basis of anatomic origin: *(a)* those arising from the ventral anlage (right-sided well-encapsulated tumors with no calcification and a good prognosis), and *(b)* those arising from the dorsal anlage (left-sided infiltrative tumors that contain islet cells and calcification, with a poor prognosis) (27). Most patients are between 1 and 8 years of age (mean, 5 years) (25,27). Pancreatoblastoma rarely occurs in adults; when it does, however, the tumor is generally more aggressive. An association of cystic pancreatoblastoma with Beckwith-Wiedemann syndrome has been reported. Pancreatoblastoma has a predilection for male patients (1.3–2.7 times more common in males than in females) and Asian individuals (>50% of cases) (25). The serum α–fetoprotein level is elevated in 25%–33% of cases (1). Pancreatoblastoma is typically slow growing and generally manifests as an asymptomatic large mass (mean, 10 cm; range, 1.5–20 cm) (25). Symptoms (when present) relate to mass effect from the tumor and include abdominal pain, early satiety, vomiting, and constipation. Cushing syndrome and syndrome of inappropriate antidiuretic hormone resulting from adrenocorticotropic hormone secretion by the tumor have been observed.

Because of the large size of the mass at presentation, in 50% of cases it is not possible to identify the organ of origin at radiology (28). Therefore, differentiation from other pediatric tumors arising from adjacent organs (eg, neuroblastoma, Wilms tumor, hepatoblastoma) is challenging, and biopsy is generally required to establish the diagnosis. Aggressive behavior with local and distant spread has been observed. Metastases may occur to the liver (the most common location), lymph nodes, lung, bone, posterior mediastinum, peritoneum, and omentum. In some cases, pancreatoblastoma may appear as a circumscribed,

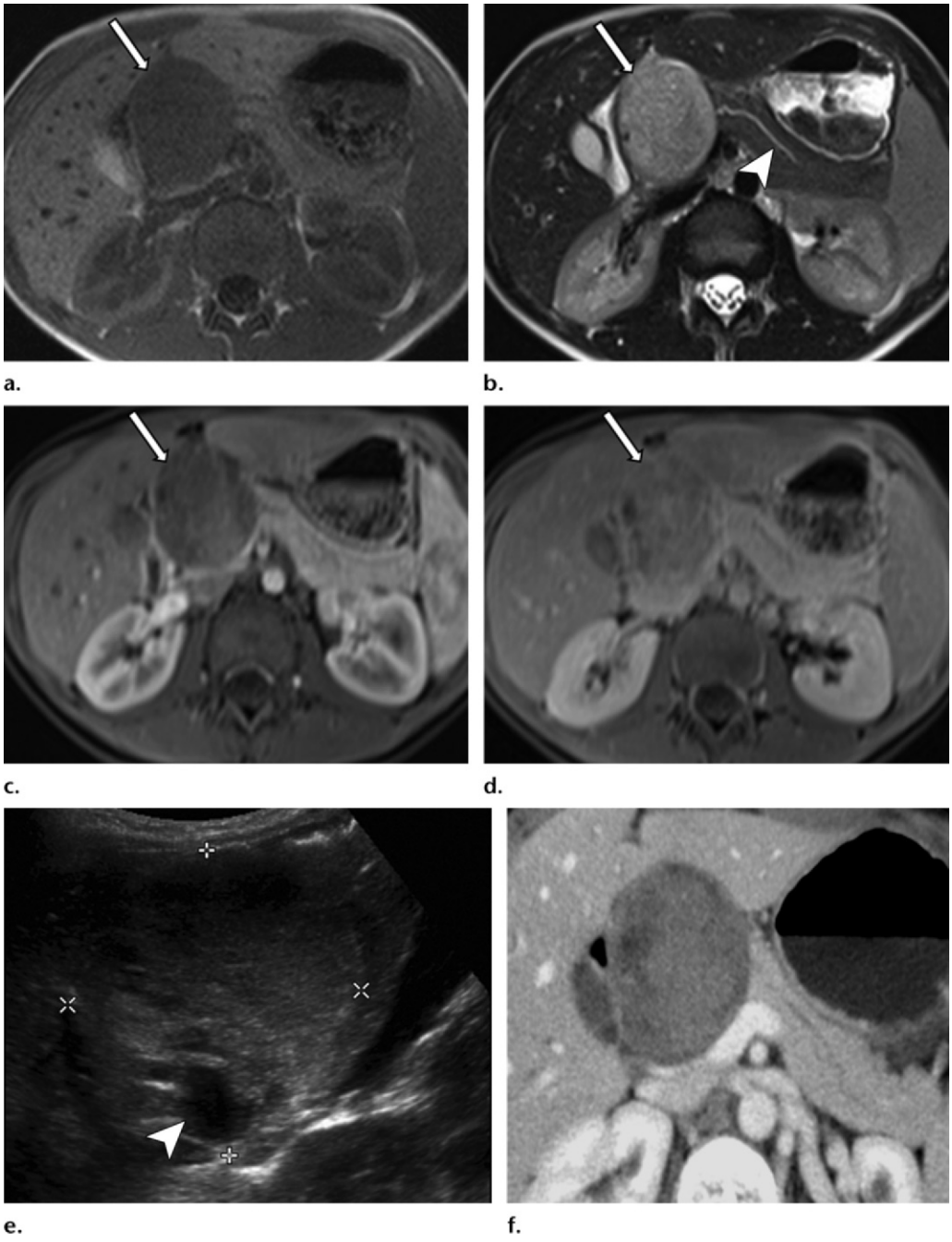

Figure 12. SPT in a 13-year-old girl with vague abdominal discomfort. **(a–d)** Axial T1-weighted **(a)**, T2-weighted **(b)**, postcontrast arterial phase T1-weighted **(c)**, and postcontrast portal phase T1-weighted **(d)** MR images show a well-encapsulated solid tumor (arrow) in the pancreatic head. The tumor has low signal intensity on the T1-weighted images and intermediate to high signal intensity on the corresponding T2-weighted image. It shows mild heterogeneous arterial enhancement with progressive nonuniform fill-in during the portal phase. Despite its large size, the tumor does not obstruct the MPD (arrowhead in **b**), which is of normal caliber. **(e, f)** Corresponding US image **(e)** and postcontrast portal phase CT scan **(f)** show the tumor with heterogeneous echogenicity and attenuation, respectively. A focal area of intratumoral cystic degeneration is seen on the US image (arrowhead in **e**).

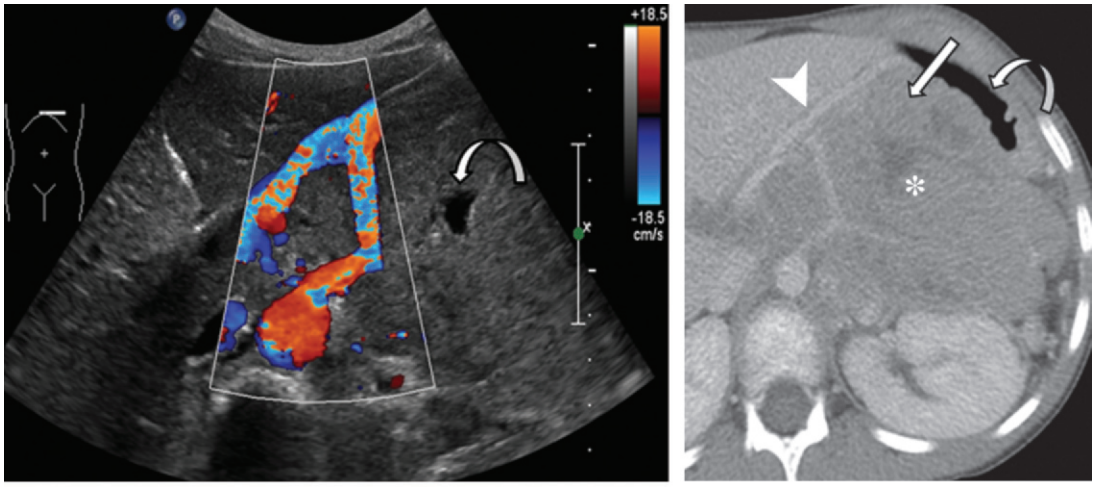

a. b.

Figure 13. Pancreatoblastoma in a 5-year-old boy in whom a mass was detected incidentally at physical examination performed during elective dental surgery. **(a)** Doppler US image shows a large heterogeneous tumor with internal cystic spaces (arrow) encasing the celiac axis and displacing the extrahepatic portal vein. **(b)** Postcontrast portal phase CT scan shows the tumor with solid (straight arrow) and cystic (*) components. The tumor displaces the portosplenic confluence (arrowhead) and stomach (curved arrow) anteriorly. Because of the large size of the tumor, the organ of origin could not be determined, and biopsy was necessary to establish the diagnosis. (Case courtesy of Harold Dhliwayo, MD, University of Alberta Hospital, Edmonton, Alberta, Canada.)

lobulated mass (with a predilection for the pancreatic head) with solid and cystic components or calcification. Despite its size, the tumor rarely causes biliary or duodenal obstruction, since it has a soft, gelatinous consistency. Arterial encasement and venous invasion have been observed (Fig 13) (25). At US, the mass is heterogeneous with hypoechoic cystic spaces (representing liquefactive necrosis) and intervening hyperechoic internal septa (25). Occasionally, a hypoechoic solid mass is seen. At CT, pancreatoblastoma generally manifests as a multiloculated inhomogeneous mass with enhancing septa (25). Calcifications (when present) have a rimlike or clustered configuration (25). The tumor has low to intermediate signal intensity on T1-weighted MR images and high signal intensity on T2-weighted images, and shows mild contrast enhancement.

Surgery is the treatment of choice. Tumors are resectable in 75% of cases, and 14% progress after resection (necessitating long-term follow-up imaging) (27). Tumors located in the pancreatic body and tail carry a poor prognosis, since they are more difficult to excise completely.

Pancreatic Lymphoma

Pancreatic lymphoma is most commonly a B-cell subtype of non-Hodgkin lymphoma and is classified as either primary or secondary. Secondary lymphoma (found in 30% of non-Hodgkin lymphoma patients with widespread disease) is the dominant form and is the result of direct extension from peripancreatic lymphadenopathy (Fig 14) (29). Primary pancreatic lymphoma is rare, representing less than 2% of extranodal lymphomas and 0.5% of pancreatic tumors (29). It is more common in middle-aged patients (mean, 55 years; range, 35–75 years) and in immunocompromised patients (eg, patients with human immunodeficiency virus, transplant recipients) (30). The clinical presentation is nonspecific, with the most common findings being abdominal pain (83% of cases), a mass (58%), and weight loss (50%) (30). Obstructive jaundice (37%–42% of cases) and acute pancreatitis (12%) are less commonly seen (30). The classic symptoms of non-Hodgkin lymphoma (eg, fever, chills, night sweats) are present in only 2% of cases.

A primary lesion of the pancreas may be difficult to distinguish from adjacent disease in the peripancreatic lymph nodes or duodenum. Ante-

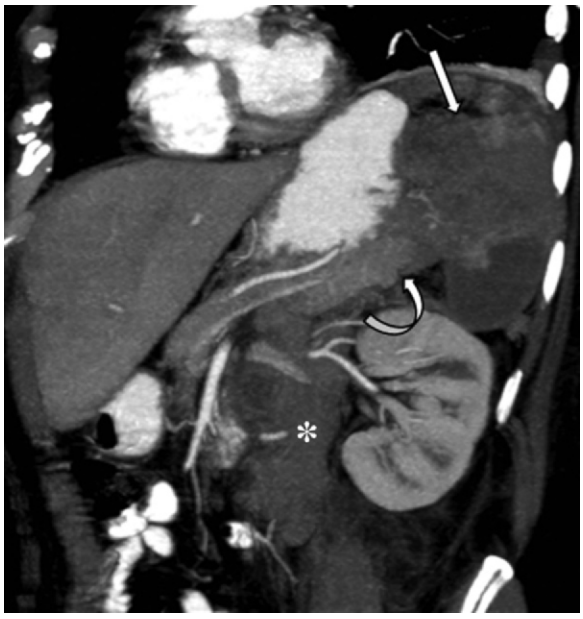

Figure 14. Secondary lymphoma of the pancreas in a 54-year-old man with abdominal pain. Coronal oblique postcontrast arterial phase maximum intensity projection image shows local invasion of the pancreatic tail (curved arrow) from lymphomatous infiltration of the spleen (straight arrow) and extensive confluent retroperitoneal lymphadenopathy (*).

Figure 15. Primary pancreatic lymphoma in a 56-year-old woman with right upper quadrant pain who had undergone renal transplantation 10 years earlier for chronic renal insufficiency (note the atrophic kidneys [*]). US showed a gallstone but failed to adequately depict the pancreas. Endoscopic retrograde cholangiopancreatography showed abrupt narrowing of the CBD, which was treated with placement of a metallic stent. Postcontrast portal phase CT scan shows a focal hypoattenuating tumor (straight arrow) in the pancreatic head, a finding that was confirmed to be lymphoma at biopsy. A gallstone (arrowhead) and the biliary stent (curved arrow) are also noted.

rior displacement of the pancreas or an intact fat plane between the pancreas and adjacent disease is a distinguishing feature. Two morphologic patterns of pancreatic lymphoma are recognized (31): a focal well-circumscribed form and a diffuse form. The focal form occurs in the pancreatic head in 80% of cases and has a mean size of 8 cm (range, 2–15 cm) (Fig 15) (30). It typically has uniform low attenuation at CT. At MR imaging, it has low signal intensity on T1-weighted images and intermediate signal intensity on T2-weighted images (slightly higher signal intensity than the pancreas but lower signal intensity than fluid), and shows faint contrast enhancement. The diffuse form is infiltrative, leading to glandular enlargement and poor definition, features that can simulate the appearance of acute pancreatitis. This form has low signal intensity on T1- and T2-weighted MR images and shows homogeneous contrast enhancement, although small foci of reduced or absent enhancement are sometimes seen.

Teaching Point

Several features of lymphoma may help distinguish it from adenocarcinoma (31).

1. A bulky localized tumor in the pancreatic head without significant MPD dilatation. The MPD is typically mildly dilated in lymphoma but grossly dilated in adenocarcinoma. CBD dilatation is more common than MPD dilatation in lymphoma.

2. Enlarged lymph nodes below the level of the renal vein.

3. Invasive tumor growth that does not respect anatomic boundaries and that infiltrates retroperitoneal or upper abdominal organs and the gastrointestinal tract.

Vascular invasion is less common in lymphoma than in adenocarcinoma. Intratumoral calcification-necrosis is not a feature of lymphoma and may be helpful in its exclusion. Biopsy is recommended for establishing the diagnosis. Pancreatic lymphoma carries a better prognosis than adenocarcinoma because first-line treatment with chemotherapy is generally effective in producing long-term disease regression or remission. Surgery is not required in most cases.

Metastases to the Pancreas

Pancreatic metastases are seen at 2%–11% of autopsies and account for 2%–5% of all malignant neoplasms (32). Metastases are most frequently from renal cell carcinoma (RCC) and lung carcinoma, followed by breast carcinoma, colorectal carcinoma, and melanoma (32). The time interval between the diagnosis of primary carcinoma and the detection of pancreatic metastases varies but is usually less than 3 years. However, metastases from RCC typically manifest 6–12 years (and as long as 20 years) after nephrectomy (33). Clinical symptoms are nonspecific and may include abdominal pain, weight loss, gastrointestinal bleeding, anemia, and diabetic ketoacidosis. Most patients (50%–83%) are asymptomatic (32). The prognosis is generally more favorable than that for pancreatic adenocarcinoma. Surgery is an option in patients who *(a)* have enjoyed a long disease-free interval between resection of primary carcinoma and the development of pancreatic metastases, or *(b)* have metastases that are confined to the pancreas. Up to 80% of patients with pancreatic metastases from RCC will have no other organ involvement (33).

Three morphologic patterns of involvement are recognized: solitary (50%–70% of cases), multifocal (5%–10%), and diffuse (15%–44%) (32,34). The solitary form is generally well marginated. Masses may be hypo- or hyperechoic at US and hypo- or isoattenuating at nonenhanced CT. Cystic masses have been reported (35). Metastases typically have low signal intensity on T1-weighted MR images and high signal intensity on T2-weighted images (36). At contrast-enhanced CT and MR imaging, the appearances of pancreatic metastases closely resemble that of primary carcinoma. Pancreatic adenocarcinoma generally manifests as a hypoenhancing mass, whereas metastases show either peripheral enhancement (in over 70% of lesions >1.5 cm) or, less commonly, homogeneous enhancement (smaller lesions) (32,35,36). These features relate to the blood supply of the lesions. Metastases parasitize the blood supply from surrounding organs, resulting in uniform enhancement in small lesions. In larger lesions, ring enhancement is the norm, since the periphery of the tumor receives more favorable blood supply than does its center. This phenomenon is typified by metastases from RCC, which are generally well-defined hypervascular lesions that have a central hypoenhancing necrotic portion with poor perfusion (Fig 16).

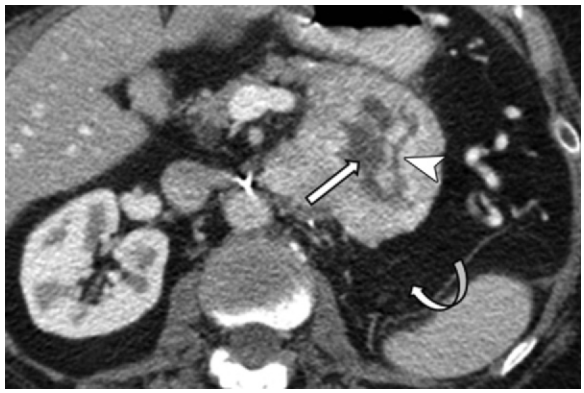

Figure 16. Pathologically proved metastasis to the pancreas from RCC in an asymptomatic 68-year-old woman who had undergone left nephrectomy 20 years earlier. Postcontrast portal phase CT scan shows a large hypervascular tumor with cystic-necrotic degeneration in the pancreatic tail (straight arrow). Arrowhead indicates intratumoral vessels, curved arrow indicates absence of left kidney.

Figure 17. Focal pancreatitis in a 33-year-old man with a long-standing history of chronic pancreatitis. Nonenhanced CT scan shows a focally enlarged pancreatic head (arrow) with an irregular convex contour and internal foci of coarse calcification. These findings remained stable at follow-up imaging performed over a 3-year period.

The main differential consideration for pancreatic metastases from hypervascular primary

tumors such as RCC is NET. The imaging appearances of these two entities can be very similar. Both manifest as hypervascular discrete masses that can exhibit cystic-necrotic degeneration. However, hypovascular metastases from (for example) the lung, breast, and colon are often seen, and the main differential consideration for these lesions (in the absence of multiple metastases) is pancreatic adenocarcinoma. In most cases, a past medical history of malignancy allows the correct diagnosis. Equivocal cases may require biopsy.

Miscellaneous Neoplastic Solid Lesions

Some exceedingly rare tumors have been described in small case series and isolated reports in the literature.

1. Epithelial tumors such as acinar cell carcinoma, giant cell tumor, and colloid carcinoma. Acinar cell carcinoma represents about 1% of all exocrine pancreatic tumors. In 10% of cases, the tumor produces excess pancreatic enzyme—notably lipase—resulting in lipase hypersecretion syndrome, which is characterized by subcutaneous fat necrosis, bone infarcts, and polyarthritis.

2. Mesenchymal tumors such as granular cell tumor, fibrous histiocytoma, juvenile hemangioendothelioma, fibroma, inflammatory myoblastic tumor, and sarcoma.

3. Mixed tumors such as squamous cell carcinoma and mixed endocrine-exocrine tumor.

Nonneoplastic Solid Lesions

Focal Pancreatitis

Chronic pancreatitis can manifest as a focal inflammatory mass, often in the pancreatic head, thereby mimicking adenocarcinoma (Fig 17). This manifestation, which is variably described in the literature as focal pancreatitis, mass-forming pancreatitis, or pseudotumoral pancreatitis, accounts for 5%–10% of pancreatectomies for presumed malignancy (37). Discrimination between focal pancreatitis and adenocarcinoma is difficult clinically, radiologically, and even histologically. Clinical features such as abdominal pain, obstructive jaundice, and weight loss may be seen in both entities. Imaging results are confusing because inflammation can coexist with adenocarcinoma and adenocarcinoma may arise in long-standing chronic pancreatitis (2% of cases after 10 years and 6% after 20 years) (38). Biopsy does not always help differentiate between the two entities, since they may share some common histologic features (39).

In general, adenocarcinoma and focal pancreatitis are hypoechoic at US, are hypoattenuating at CT, and have the same signal intensity at T1- and T2-weighted MR imaging. The double duct sign, ductal strictures, infiltration of adjacent fat, arterial encasement, and peripancreatic venous obstruction may be present in both entities (39). Features that favor a diagnosis of focal pancreatitis include nondilated or smoothly tapering pancreatic and bile ducts coursing through the mass ("duct penetrating sign" [40]), pancreatic duct irregularity, and the presence of pancreatic calcifications (39). Features that favor a diagnosis of adenocarcinoma include abrupt interruption of a smoothly dilated pancreatic duct and upstream pancreatic gland atrophy (39). A high ratio of duct caliber to pancreatic gland width is a recognized indicator of adenocarcinoma (39). Modest atrophy and nonabrupt gradual narrowing of the biliary or pancreatic duct is more common in focal pancreatitis (39).

Autoimmune pancreatitis (AIP) is a distinct form of pancreatitis that accounts for 25% of all cases of focal pancreatitis (41). Its importance lies in the fact that laboratory and imaging findings may improve following a course of treatment with corticosteroids. AIP is characterized by a lymphoplasmacytic infiltrate at histologic analysis, an elevated serum level of immunoglobulin G4, and an association with other autoimmune conditions such as inflammatory bowel disease, primary sclerosing cholangitis, and Sjögren syndrome (41). At imaging, diffuse AIP typically shows generalized glandular enlargement ("sausage" shape), loss of visualization of the MPD due to the destructive nature of this disease entity, and a rimlike capsule due to fibrosis (41). Focal AIP is more difficult to distinguish from adenocarcinoma (Figs 18, 19). At endoscopic retrograde cholangiopancreatography, stenosis of a segment of the MPD greater than 3 cm in length and an upstream portion of the MPD less than 0.6 cm in diameter are reported to be suggestive of AIP (42).

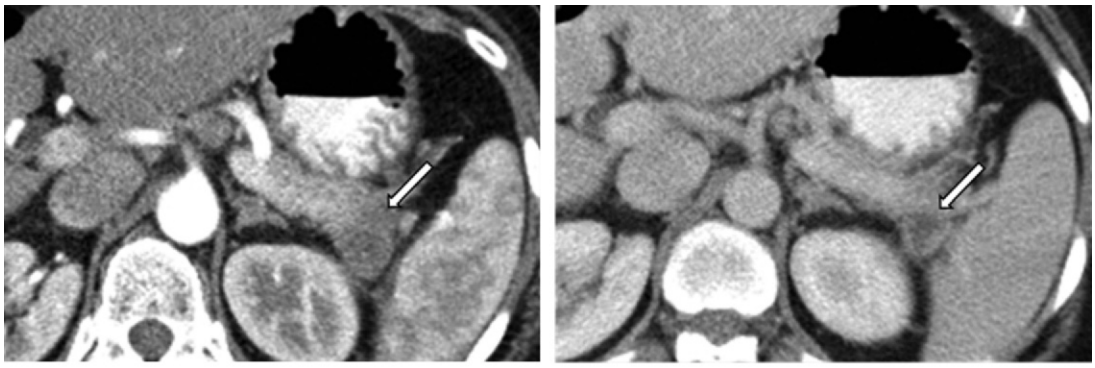

a. b.

Figure 18. Focal AIP in a 47-year-old woman with vague abdominal symptoms. Postcontrast arterial phase **(a)** and portal phase **(b)** CT scans show a focal area of hypoattenuation (arrow) in the pancreatic tail, for which the patient underwent distal pancreatectomy for presumed adenocarcinoma. Pathologic analysis of the resected specimen revealed AIP.

Groove pancreatitis is an uncommon form of focal pancreatitis, and its cause is unknown. The pancreaticoduodenal groove is a potential space between the pancreatic head, duodenum, and CBD. There are two forms of groove pancreatitis (43): *(a)* the segmental form, which involves the pancreatic head with scar tissue in the pancreaticoduodenal groove; and *(b)* the pure form, which affects the groove but spares the pancreatic head. Clinical manifestations generally relate to associated duodenal and biliary obstruction, with recurrent vomiting being particularly pronounced due to duodenal obstruction. At imaging, sheetlike fibrotic scar tissue is seen in the pancreaticoduodenal groove and is typically hypoattenuating at CT, hypointense at T1-weighted MR imaging, and iso- to hyperintense at T2-weighted imaging (43). The fibrotic scar tissue shows delayed enhancement at contrast-enhanced CT and MR imaging. The segmental form, which involves both the pancreatic head and the pancreaticoduodenal groove, may resemble a focal mass at imaging, thereby mimicking adenocarcinoma. Groove pancreatitis is associated with *(a)* smooth stricturing of the intrapancreatic portion of the CBD, and *(b)* wall thickening and cystic dysplasia of the duodenum (43).

The literature contains conflicting reports regarding the helpfulness of contrast enhancement in differentiating pancreatitis from adenocarcinoma. Earlier studies suggested that the two entities cannot be differentiated on the basis of enhancement, since both show delayed enhancement at CT and MR imaging secondary to fibrosis (44,45). However, more recent studies suggest otherwise (37,46). Tajima et al (37) suggest that analysis of signal intensity curves at contrast-enhanced MR

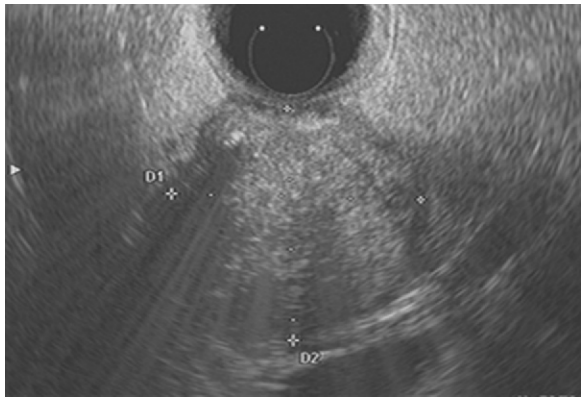

Figure 19. Focal AIP. Endoscopic US image shows a focal heterogeneous mass (cursors) in the pancreatic head. Endoscopic US–guided fine needle aspiration biopsy revealed AIP. (Courtesy of Gurpal Sandha, MD, University of Alberta Hospital, Edmonton, Alberta, Canada.)

imaging is useful because adenocarcinoma has a later enhancement peak than does focal pancreatitis (a slow rise to a peak at 180 seconds was unique to adenocarcinoma in their study). Yamada et al (46) found that analysis of time attenuation curves at contrast-enhanced CT allowed differentiation between the two entities: Focal pancreatitis showed a delayed washout pattern, whereas adenocarcinoma showed a pattern of increasing enhancement over time, peaking at 150 seconds.

Diffusion-weighted MR imaging and FDG PET have shown early promise in differentiating focal pancreatitis from adenocarcinoma. Tumors are associated with restricted diffusion due to their dense cellularity and therefore generally have higher signal intensity and lower apparent diffusion coefficient values than does normal tissue at diffusion-weighted MR imaging. In a diffusion-weighted MR imaging study of 38 patients, Fattahi

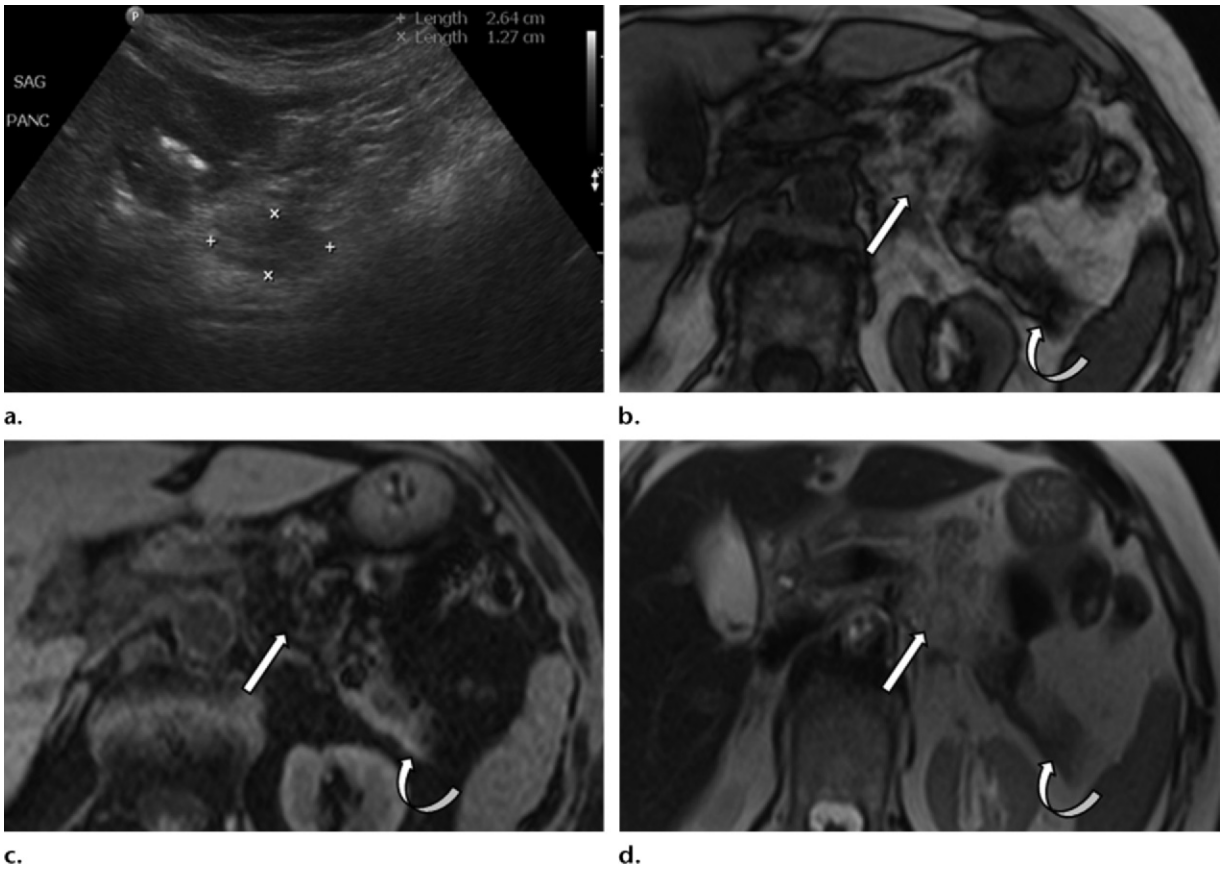

Figure 20. Diffuse nonuniform fatty replacement of the pancreas with focal sparing in a 45-year-old woman with right upper quadrant pain. **(a)** US image shows a focal hypoechoic area (cursors) representing focal sparing in a diffusely echogenic (fatty) pancreas. **(b–d)** Axial opposed-phase T1-weighted **(b)**, fat-suppressed T1-weighted **(c)**, and T2-weighted **(d)** MR images show diffuse nonuniform fatty replacement of the pancreas (straight arrow) with interspersed focal areas of sparing (curved arrow). The areas of fatty replacement are hyperintense on the non–fat-suppressed T1- and T2-weighted MR images and show signal intensity loss on the fat-suppressed image. The focal areas of sparing are hypointense relative to the fatty pancreas on the non–fat-suppressed T1- and T2-weighted images.

et al (47) found that, at a *b* value of 600 sec/mm^2, focal pancreatitis was indistinguishable from the remaining pancreas, whereas adenocarcinoma was hyperintense relative to the remaining pancreas. The mean apparent diffusion coefficient value for adenocarcinoma ($1.46 \pm 0.18 \times 10^{-3}$ mm^2/sec) was significantly lower than that for focal pancreatitis ($2.09 \pm 0.18 \times 10^{-3}$ mm^2/sec) or normal pancreatic tissue ($1.78 \pm 0.07 \times 10^{-3}$ mm^2/sec). FDG PET has also yielded encouraging results in differentiating adenocarcinoma from focal pancreatitis. In a series of 80 patients, Friess et al (48) reported increased uptake in 41 of 42 patients (98%) with adenocarcinoma and no accumulation in 28 of 32 patients (88%) with chronic pancreatitis.

Fatty Infiltration-Replacement

Pancreatic lipomatosis, or fatty infiltration-replacement, is a common finding in the adult pancreas. Involvement is normally diffuse but may in rare instances be focal. It is most frequently seen in elderly or obese patients and may be associated with diseases such as chronic pancreatitis and cystic fibrosis. A geographic predilection for the anterior aspect of the pancreatic head has been observed. The posterior part of the head and the uncinate process are usually spared from fatty infiltration. The differences in the geographic distribution of fatty infiltration-replacement and sparing are postulated to relate to the dissimilar histologic compositions of the ventral and dorsal pancreas (49).

Focal fatty infiltration and its converse, focal fatty sparing, may each simulate a tumor. At US, focal fatty infiltration is hyperechoic relative to the normal pancreas, whereas focal fatty sparing is hypoechoic relative to the surrounding fatty pancreas (Fig 20a). Nonenhanced CT can suggest the diagnosis if the lesion contains sufficient

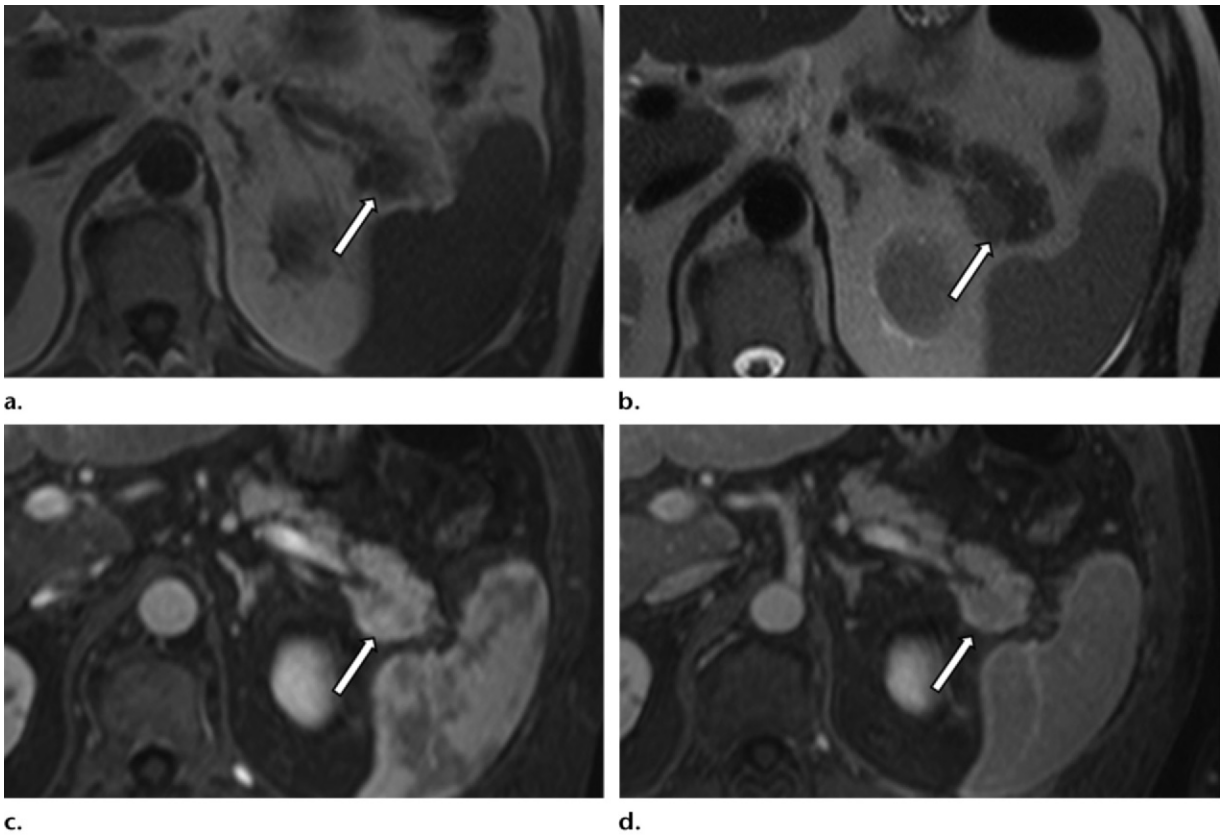

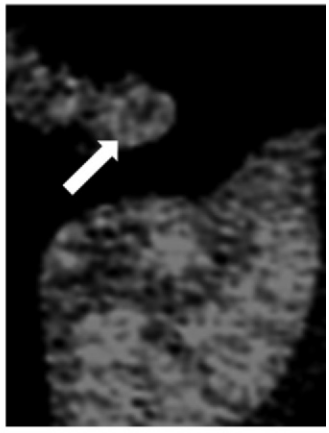

Figure 21. IPAS in a 34-year-old man with a past history of a resected duodenal carcinoid tumor. **(a–d)** Axial T1-weighted **(a)**, T2-weighted **(b)**, and postcontrast arterial phase **(c)** and portal phase **(d)** T1-weighted MR images show a small ovoid mass (arrow) in the pancreatic tail. The mass has signal intensity similar to that of the spleen with all imaging sequences and demonstrates the characteristic arciform arterial enhancement of splenic tissue **(c)**. The MR imaging findings are consistent with a diagnosis of IPAS. **(e)** Postcontrast arterial phase CT scan also shows the mass with arciform arterial enhancement (arrow). ^{99m}Tc heat-damaged red blood cell (HDRBC) SPECT/CT was recommended to confirm the diagnosis.

macroscopic fat to exhibit characteristic fat attenuation (in negative Hounsfield units) (49). Contrast-enhanced CT is seldom helpful because normal parenchyma interspersed between foci of fatty infiltration enhances, increasing lesion attenuation beyond that which is diagnostic for fat (49). The absence of mass effect is a useful ancillary finding that may help differentiate focal fatty infiltration and focal fatty sparing from tumor. Nondeformity of the configuration of the pancreas and absence of associated ductal or vascular displacement in the affected area are typical (49).

MR imaging is the modality of choice for assessment due to its high specificity in the detection of fat (Fig 20b–20d) (50,51). Macroscopic fatty replacement of the pancreas will demonstrate signal intensity similar to that of fat found elsewhere in the body (ie, high signal with T1- and T2-weighted sequences, signal loss with fat-suppressed sequences). Microscopic fat, which is commonly present in fatty infiltration, is reliably detected with use of chemical shift MR imaging. Involved areas show moderate to marked signal loss with the opposed-phase T1-weighted sequence relative to the in-phase T1-weighted sequence.

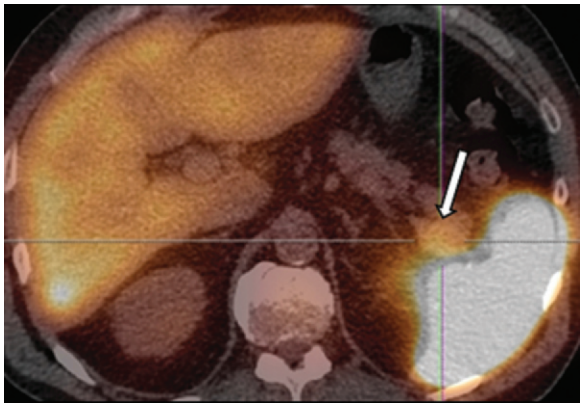

Figure 22. Confirmation of the diagnosis of IPAS in the same patient as in Figure 21. Axial fused ^{99m}Tc HDRBC SPECT/CT image shows focal uptake (arrow) in the pancreatic tail, a finding that is consistent with IPAS. However, this uptake is lower than in the spleen because the IPAS contains only a small amount of functioning splenic tissue.

Intrapancreatic Accessory Spleen

Accessory spleen occurs as a result of failure of fusion of the splenic anlage in the dorsal mesogastrium (52). It is seen at 10%–30% of autopsies, with the pancreatic tail being the second most common location (52). However, intrapancreatic accessory spleen (IPAS) is seldom detected at imaging due to its small size. Mortele et al (52) reported a prevalence of two cases per 1000 patients on the basis of findings at nonenhanced and contrast-enhanced portal phase CT (8-mm collimation, pitch of 1).

IPAS is typically a 1–3-cm, well-defined ovoid mass situated in the pancreatic tail. It is homogeneous and mildly echogenic at US and may exhibit posterior acoustic enhancement (53). A vascular hilum passing into the lesion is reported to be a suggestive finding at color Doppler US (53). IPAS has characteristics similar to those of the spleen at nonenhanced and contrast-enhanced imaging (Fig 21) (53). Relative to the spleen, IPAS is isoechoic at US, isoattenuating at CT, and isointense at MR imaging. Because the spleen is generally more dense than the pancreas during all dynamic CT phases (arterial, pancreatic, portal), IPAS generally shows greater enhancement than does the pancreas. Relative to the pancreas, IPAS (like the spleen) has lower signal intensity on T1-weighted MR images and higher signal intensity on T2-weighted images. The characteristic arciform splenic enhancement pattern seen during the arterial phase (secondary to perfusion differences between red and white pulp) is also seen in IPAS. This is a useful criterion for differentiating IPAS from hypervascular neoplasms such as NETs and metastases. Superparamagnetic iron oxide–enhanced MR imaging is useful for confirming the diagnosis of IPAS in equivocal cases (54). Superparamagnetic iron oxide is selectively phagocytosed by macrophages of reticuloendothelial cells in splenic tissue, liver, and bone marrow, leading to decreased signal in these tissues at postcontrast imaging, with the signal decrease of IPAS matching that of the spleen.

Technetium 99m (^{99m}Tc) sulfur colloid scintigraphy and ^{99m}Tc HDRBC scintigraphy can be used to confirm the diagnosis when IPAS is suspected (Fig 22) (53). Splenic tissue traps up to 90% of the injected HDRBCs, thereby making ^{99m}Tc HDRBC scintigraphy a highly sensitive modality. However, this modality is more time consuming than ^{99m}Tc sulfur colloid scintigraphy and requires direct handling of the blood products. False-negative findings may be obtained if only a minimal amount of functioning splenic tissue is present. Diagnostic criteria used to detect accessory spleen, including IPAS, include *(a)* a marked increase in uptake that exceeds that of the cardiac blood pool, and *(b)* major vessels at the site of a suspected accessory spleen (53).

Pancreatic Lobulation and Other Congenital Anomalies

The normal pancreas has a lobulated appearance. Occasionally, however, a prominent focal exophytic lobulation (generally an outpouching of more than 1 cm beyond the pancreatic border) may simulate a pancreatic mass. Lobulations are most commonly located in the pancreatic head and neck and are present in about 34% of the general population. Ross et al (55) classified these lobulations into three types: type I (anterior [10% of cases]), type II (posterior [19%]), and type III (horizontal [5%]). Type I lobulations are often associated with a smaller uncinate process. Tuber omentale, a focal prominence of the anterior surface of the pancreatic body to the left of the superior mesenteric vessels, is another example of a pseudotumor (56), as is bifid pancreatic tail (pancreas bifidum), or fish tail pancreas, a very rare congenital branching anomaly of the MPD that is identified at MR cholangiopancreatography or endoscopic retrograde cholangiopancreatography

Teaching Point

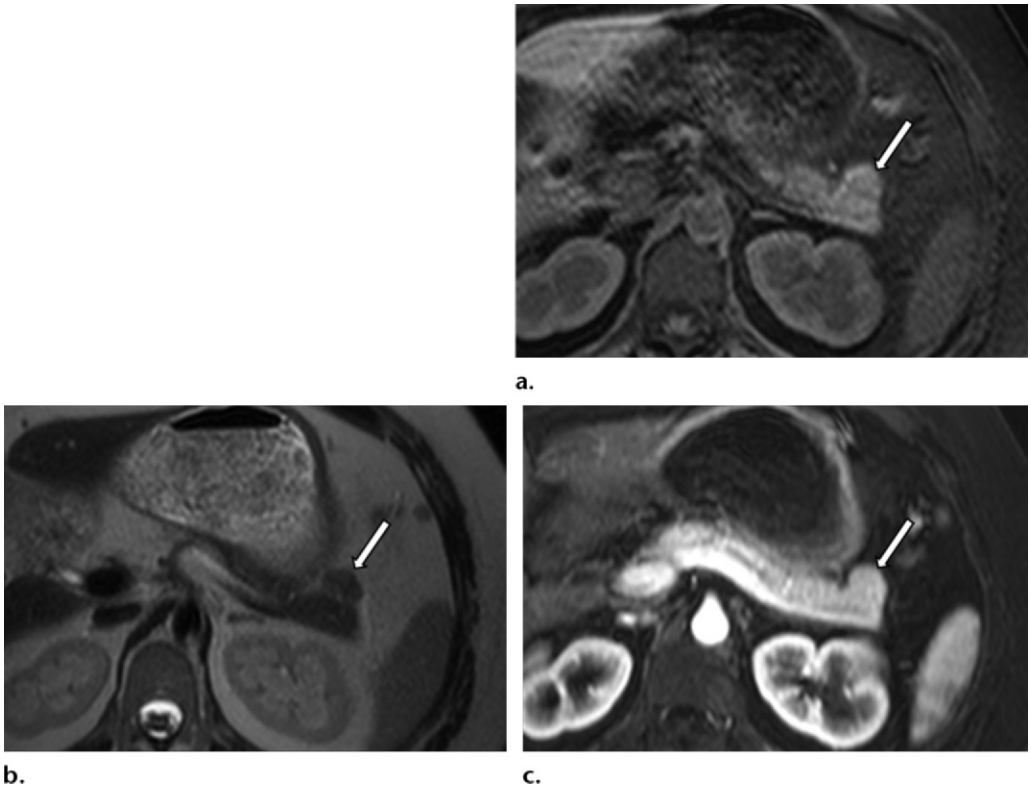

Figure 23. Prominent pancreatic lobulation in a 44-year-old woman in whom a misdiagnosis (tumor of the pancreatic tail) was made at US. Axial fat-suppressed T1-weighted **(a)**, T2-weighted **(b)**, and postcontrast arterial phase T1-weighted **(c)** MR images show a well-defined exophytic focal mass (arrow) that is isointense relative to the surrounding pancreas, a finding that is consistent with pancreatic lobulation.

and is associated with division of the pancreatic tail into separate dorsal and ventral buds (57). The pancreatic tail does not tend to reach the splenic hilum when these anomalies occur, a telltale sign of their presence.

At imaging, lobulations can be distinguished from tumor in that their characteristics are identical to those of the rest of the pancreas. Relative to the surrounding pancreatic tissue, lobulations are isoechoic at US, isoattenuating at CT, and isointense at MR imaging, and are isoenhancing following contrast material administration (Fig 23).

Miscellaneous Non-neoplastic Solid Lesions

Pancreatic Sarcoidosis.—Sarcoidosis is an idiopathic systemic granulomatous disorder that can affect any organ in the body. Pancreatic involvement is very rare, however, with only 19 cases of biopsy-proved granuloma of the pancreas and seven cases of peripancreatic lymph node involvement reported in the literature (58). Pancreatic sarcoidosis can mimic pancreatic adenocarcinoma both clinically and radiologically (59). Abdominal pain, weight loss, and obstructive jaundice are the most common presenting symptoms (60). Sarcoidosis may manifest as solitary or multiple pancreatic masses that may reach 6–7 cm in size (61). Coexisting peripancreatic lymph node enlargement has been described (61). Sarcoid lesions are typically hypoechoic at US and hypoattenuating at contrast-enhanced CT (61). A geographic predilection for the pancreatic head has been reported, a finding that may be associated with obstruction of the CBD and MPD (61). CBD narrowing from sarcoidosis is typically long, smooth, and tapered as opposed to focally abrupt (as in adenocarcinoma) (61). At MR imaging, sarcoid lesions are hypointense on T1-weighted images, mildly hyperintense on T2-weighted images, and hypoenhancing following contrast material administration (60).

The presence of a pancreatic mass in a patient with a history of sarcoidosis or with typical pulmonary findings such as bilateral hilar adenopathy should alert the radiologist to the possibility of pancreatic sarcoidosis. Nevertheless, biopsy is recommended in all cases. The prognosis is good because pancreatic sarcoidosis is generally responsive to steroid treatment (60,61).

Castleman Disease of the Pancreas.—Castleman disease was first described by Castleman and Towne in 1956 and is a rare, angiofollicular lymph node hyperplasia of unknown origin (62). It is most commonly seen in the mediastinum but may occur at any site where lymph nodes exist (63). Pancreatic involvement is exceedingly rare, with only 10 cases reported in the literature (64). At CT, Castleman disease has been reported to manifest as a solid, well-encapsulated smooth mass with strong contrast enhancement, which may be ringlike (63). Internal calcification and cystic change have also been described (65,66). The one reported case involving MR imaging describes a smoothly marginated mass that is hypointense at T1-weighted imaging and isointense at T2-weighted imaging, with peripheral arterial rim enhancement following contrast material administration (67).

Conclusions

Solid lesions of the pancreas can have a broad spectrum of neoplastic and nonneoplastic causes. Accurate diagnosis can be challenging, and a multimodality imaging approach is often helpful. Knowledge of relevant clinical information and key radiologic features is essential for confident lesion characterization and differentiation.

References

1. Winter JM, Cameron JL, Lillemoe KD, et al. Periampullary and pancreatic incidentaloma: a single institution's experience with an increasingly common diagnosis. Ann Surg 2006;243(5):673–680; discussion 680–683.
2. Ros PR, Mortelé KJ. Imaging features of pancreatic neoplasms. JBR-BTR 2001;84(6):239–249.
3. Brennan DD, Zamboni GA, Raptopoulos VD, Kruskal JB. Comprehensive preoperative assessment of pancreatic adenocarcinoma with 64-section volumetric CT. RadioGraphics 2007;27(6): 1653–1666.
4. Tempero M, Arnoletti JP, Behrman S, et al. Clinical Practice Guidelines in Oncology: pancreatic adenocarcinoma. National Comprehensive Cancer Network. 2010; version 2. Available at: http://www.nccn.org/. Accessed July 2010.
5. Lu DS, Reber HA, Krasny RM, Kadell BM, Sayre J. Local staging of pancreatic cancer: criteria for unresectability of major vessels as revealed by pancreatic-phase, thin-section helical CT. AJR Am J Roentgenol 1997;168(6):1439–1443.
6. Hough TJ, Raptopoulos V, Siewert B, Matthews JB. Teardrop superior mesenteric vein: CT sign for unresectable carcinoma of the pancreas. AJR Am J Roentgenol 1999;173(6):1509–1512.
7. Kosmahl M, Pauser U, Anlauf M, Klöppel G. Pancreatic ductal adenocarcinomas with cystic features: neither rare nor uniform. Mod Pathol 2005; 18(9):1157–1164.
8. Hanbidge AE. Cancer of the pancreas: the best image for early detection—CT, MRI, PET or US? Can J Gastroenterol 2002;16(2):101–105.
9. DeWitt J, Devereaux B, Chriswell M, et al. Comparison of endoscopic ultrasonography and multidetector computed tomography for detecting and staging pancreatic cancer. Ann Intern Med 2004;141(10):753–763.
10. Inokuma T, Okamoto T, Ogami T, et al. Diagnosis of pancreatic cancer with FDG-PET: comparison with CT, US and endoscopic US [abstr]. Gut 1996; 39(suppl 3):12.
11. Berberat P, Friess H, Kashiwagi M, Beger HG, Büchler MW. Diagnosis and staging of pancreatic cancer by positron emission tomography. World J Surg 1999;23(9):882–887.
12. Fröhlich A, Diederichs CG, Staib L, Vogel J, Beger HG, Reske SN. Detection of liver metastases from pancreatic cancer using FDG PET. J Nucl Med 1999;40(2):250–255.
13. Oberg K, Eriksson B. Endocrine tumours of the pancreas. Best Pract Res Clin Gastroenterol 2005; 19(5):753–781.
14. Noone TC, Hosey J, Firat Z, Semelka RC. Imaging and localization of islet-cell tumours of the pancreas on CT and MRI. Best Pract Res Clin Endocrinol Metab 2005;19(2):195–211.
15. Gouya H, Vignaux O, Augui J, et al. CT, endoscopic sonography, and a combined protocol for preoperative evaluation of pancreatic insulinomas. AJR Am J Roentgenol 2003;181(4):987–992.
16. Owen NJ, Sohaib SA, Peppercorn PD, et al. MRI of pancreatic neuroendocrine tumours. Br J Radiol 2001;74(886):968–973.
17. Thoeni RF, Mueller-Lisse UG, Chan R, Do NK, Shyn PB. Detection of small, functional islet cell tumors in the pancreas: selection of MR imaging sequences for optimal sensitivity. Radiology 2000; 214(2):483–490.
18. Ricke J, Klose KJ, Mignon M, Oberg K, Wiedenmann B. Standardisation of imaging in neuroendocrine tumours: results of a European delphi process. Eur J Radiol 2001;37(1):8–17.
19. Franz VK. Tumors of the pancreas. In: Atlas of tumor pathology, fasc 27–28, ser 7. Washington, DC: Armed Forces Institute of Pathology, 1959; 32–33.

20. Adams AL, Siegal GP, Jhala NC. Solid pseudopapillary tumor of the pancreas: a review of salient clinical and pathologic features. Adv Anat Pathol 2008;15(1):39–45.
21. Buetow PC, Buck JL, Pantongrag-Brown L, Beck KG, Ros PR, Adair CF. Solid and papillary epithelial neoplasm of the pancreas: imaging-pathologic correlation on 56 cases. Radiology 1996;199(3):707–711.
22. Al-Qahtani S, Gudinchet F, Laswed T, et al. Solid pseudopapillary tumor of the pancreas in children: typical radiological findings and pathological correlation. Clin Imaging 2010;34(2):152–156.
23. Yao X, Ji Y, Zeng M, Rao S, Yang B. Solid pseudopapillary tumor of the pancreas: cross-sectional imaging and pathologic correlation. Pancreas 2010;39(4):486–491.
24. Cantisani V, Mortele KJ, Levy A, et al. MR imaging features of solid pseudopapillary tumor of the pancreas in adult and pediatric patients. AJR Am J Roentgenol 2003;181(2):395–401.
25. Chung EM, Travis MD, Conran RM. Pancreatic tumors in children: radiologic-pathologic correlation. RadioGraphics 2006;26(4):1211–1238.
26. Sheng L, Weixia Z, Longhai Y, Jinming Y. Clinical and biologic analysis of pancreatoblastoma. Pancreas 2005;30(1):87–90.
27. Papaioannou G, Sebire NJ, McHugh K. Imaging of the unusual pediatric 'blastomas'. Cancer Imaging 2009;9:1–11.
28. Montemarano H, Lonergan GJ, Bulas DI, Selby DM. Pancreatoblastoma: imaging findings in 10 patients and review of the literature. Radiology 2000;214(2):476–482.
29. Zucca E, Roggero E, Bertoni F, Cavalli F. Primary extranodal non-Hodgkin's lymphomas. I. Gastrointestinal, cutaneous and genitourinary lymphomas. Ann Oncol 1997;8(8):727–737.
30. Nayer H, Weir EG, Sheth S, Ali SZ. Primary pancreatic lymphomas: a cytopathologic analysis of a rare malignancy. Cancer 2004;102(5):315–321.
31. Merkle EM, Bender GN, Brambs HJ. Imaging findings in pancreatic lymphoma: differential aspects. AJR Am J Roentgenol 2000;174(3):671–675.
32. Tsitouridis I, Diamantopoulou A, Michaelides M, Arvanity M, Papaioannou S. Pancreatic metastases: CT and MRI findings. Diagn Interv Radiol 2010;16(1):45–51.
33. Merkle EM, Boaz T, Kolokythas O, Haaga JR, Lewin JS, Brambs HJ. Metastases to the pancreas. Br J Radiol 1998;71(851):1208–1214.
34. Muranaka T, Teshima K, Honda H, Nanjo T, Hanada K, Oshiumi Y. Computed tomography and histologic appearance of pancreatic metastases from distant sources. Acta Radiol 1989;30(6):615–619.
35. Kelekis NL, Semelka RC, Siegelman ES. MRI of pancreatic metastases from renal cancer. J Comput Assist Tomogr 1996;20(2):249–253.
36. Klein KA, Stephens DH, Welch TJ. CT characteristics of metastatic disease of the pancreas. RadioGraphics 1998;18(2):369–378.
37. Tajima Y, Kuroki T, Tsutsumi R, Isomoto I, Uetani M, Kanematsu T. Pancreatic carcinoma coexisting with chronic pancreatitis versus tumor-forming pancreatitis: diagnostic utility of the time-signal intensity curve from dynamic contrast-enhanced MR imaging. World J Gastroenterol 2007;13(6):858–865.
38. Lowenfels AB, Maisonneuve P, Cavallini G, et al. Pancreatitis and the risk of pancreatic cancer. International Pancreatitis Study Group. N Engl J Med 1993;328(20):1433–1437.
39. Siddiqi AJ, Miller F. Chronic pancreatitis: ultrasound, computed tomography, and magnetic resonance imaging features. Semin Ultrasound CT MR 2007;28(5):384–394.
40. Ichikawa T, Sou H, Araki T, et al. Duct-penetrating sign at MRCP: usefulness for differentiating inflammatory pancreatic mass from pancreatic carcinomas. Radiology 2001;221(1):107–116.
41. Chang WI, Kim BJ, Lee JK, et al. The clinical and radiological characteristics of focal mass-forming autoimmune pancreatitis: comparison with chronic pancreatitis and pancreatic cancer. Pancreas 2009;38(4):401–408.
42. Wakabayashi T, Kawaura Y, Satomura Y, et al. Clinical and imaging features of autoimmune pancreatitis with focal pancreatic swelling or mass formation: comparison with so-called tumor-forming pancreatitis and pancreatic carcinoma. Am J Gastroenterol 2003;98(12):2679–2687.
43. Shanbhogue AK, Fasih N, Surabhi VR, Doherty GP, Shanbhogue DK, Sethi SK. A clinical and radiologic review of uncommon types and causes of pancreatitis. RadioGraphics 2009;29(4):1003–1026.

44. Johnson PT, Outwater EK. Pancreatic carcinoma versus chronic pancreatitis: dynamic MR imaging. Radiology 1999;212(1):213–218.
45. Kim T, Murakami T, Takamura M, et al. Pancreatic mass due to chronic pancreatitis: correlation of CT and MR imaging features with pathologic findings. AJR Am J Roentgenol 2001;177(2):367–371.
46. Yamada Y, Mori H, Matsumoto S, Kiyosue H, Hori Y, Hongo N. Pancreatic adenocarcinoma versus chronic pancreatitis: differentiation with triple-phase helical CT. Abdom Imaging 2010;35(2): 163–171.
47. Fattahi R, Balci NC, Perman WH, et al. Pancreatic diffusion-weighted imaging (DWI): comparison between mass-forming focal pancreatitis (FP), pancreatic cancer (PC), and normal pancreas. J Magn Reson Imaging 2009;29(2):350–356.
48. Friess H, Langhans J, Ebert M, et al. Diagnosis of pancreatic cancer by 2[18F]-fluoro-2-deoxy-D-glucose positron emission tomography. Gut 1995;36 (5):771–777.
49. Kawamoto S, Siegelman SS, Bluemke DA, Hruban RH, Fishman EK. Focal fatty infiltration in the head of the pancreas: evaluation with multidetector computed tomography with multiplanar reformation imaging. J Comput Assist Tomogr 2009;33(1): 90–95.
50. Kim HJ, Byun JH, Park SH, et al. Focal fatty replacement of the pancreas: usefulness of chemical shift MRI. AJR Am J Roentgenol 2007;188(2): 429–432.
51. Isserow JA, Siegelman ES, Mammone J. Focal fatty infiltration of the pancreas: MR characterization with chemical shift imaging. AJR Am J Roentgenol 1999;173(5):1263–1265.
52. Mortelé KJ, Mortelé B, Silverman SG. CT features of the accessory spleen. AJR Am J Roentgenol 2004;183(6):1653–1657.
53. Kim SH, Lee JM, Han JK, et al. Intrapancreatic accessory spleen: findings on MR imaging, CT, US and scintigraphy, and the pathologic analysis. Korean J Radiol 2008;9(2):162–174.
54. Herédia V, Altun E, Bilaj F, Ramalho M, Hyslop BW, Semelka RC. Gadolinium- and superparamagnetic-iron-oxide-enhanced MR findings of intrapancreatic accessory spleen in five patients. Magn Reson Imaging 2008;26(9):1273–1278.
55. Ross BA, Jeffrey RB Jr, Mindelzun RE. Normal variations in the lateral contour of the head and neck of the pancreas mimicking neoplasm: evaluation with dual-phase helical CT. AJR Am J Roentgenol 1996;166(4):799–801.
56. Mortelé KJ, Rocha TC, Streeter JL, Taylor AJ. Multimodality imaging of pancreatic and biliary congenital anomalies. RadioGraphics 2006;26(3): 715–731.
57. Dinter D, Löhr JM, Neff KW. Bifid tail of the pancreas: benign bifurcation anomaly. AJR Am J Roentgenol 2007;189(5):W251–W253.
58. Wijkstrom M, Bechara RI, Sarmiento JM. A rare non-malignant mass of the pancreas: case report and review of pancreatic sarcoidosis. Am Surg 2010; 76(1):79–84.
59. Soyer P, Gottlieb L, Bluemke DA, Fishman E. Sarcoidosis of the pancreas mimicking pancreatic cancer: CT features. Eur J Radiol 1994;19(1):32–33.
60. Baroni RH, Pedrosa I, Tavernaraki E, Goldsmith J, Rofsky NM. Pancreatic sarcoidosis: MRI features. J Magn Reson Imaging 2004;20(5):889–893.
61. Warshauer DM, Lee JK. Imaging manifestations of abdominal sarcoidosis. AJR Am J Roentgenol 2004; 182(1):15–28.
62. Castleman B, Iverson L, Menendez VP. Localized mediastinal lymph node hyperplasia resembling thymoma. Cancer 1956;9(4):822–830.
63. Chaulin B, Pontais C, Laurent F, De Mascarel A, Drouillard J. Pancreatic Castleman disease: CT findings. Abdom Imaging 1994;19(2):160–161.
64. Tunru-Dinh VW, Ghani A, Tom YD. Rare case of Castleman disease involving the pancreas. Am Surg 2007;73(12):1284–1287.
65. Campra D, Farina EC, Resegotti A, et al. Castleman disease in differential diagnosis of a pancreatic mass. Eur J Surg 2002;168(12):744–746.
66. Wasielica-Berger J, Kaniewska M, Cepowicz D, Wereszczynska-Siemiatkowska U, Kedra B, Dabrowski A. Castleman disease imitating pancreatic tumor presenting with pericardial and pleural effusion. Pancreas 2007;35(4):382–384.
67. Soler R, Rodríguez E, Bello MJ, Alvarez M. Pancreatic Castleman's disease: MR findings. Eur Radiol 2003;13(suppl 4):L48–L50.

RadioGraphics

Multimodality Imaging of Neoplastic and Nonneoplastic Solid Lesions of the Pancreas

Gavin Low, MBChB, MRCS, FRCR • Anukul Panu, MD • Noam Millo, MD • Edward Leen, MD, FRCR

RadioGraphics 2011; 31:993–1015 • **Published online** 10.1148/rg.314105731 • **Content Codes:** GI OI

Page 995
High-resolution dual-phase (arterial and portal) contrast material–enhanced CT is the established technique for evaluating pancreatic adenocarcinoma. Arterial phase imaging (performed 20–40 seconds after contrast agent injection) allows optimal visualization of the tumor and peripancreatic arteries. Maximal contrast between the hypovascular tumor and the normal pancreas yields optimal tumor conspicuity in this phase. Most tumors are hypoattenuating, with a mean size of 3 cm (range, 1.5–10 cm; average size in the pancreatic head, 2.5–3 cm; average size in the body and tail, 5–7 cm) (2). Portal phase imaging (performed 50–70 seconds after injection) is optimal for detecting metastatic disease to the liver and for assessing the peripancreatic veins.

Page 998 (Figure on page 1000)
The most distinctive feature of NETs is their behavior at contrast-enhanced imaging. NETs have a rich vascular supply and therefore enhance avidly during the arterial phase, enhancing more rapidly and intensely than the normal pancreas (Fig 9a, 9b) (14).

Page 1002 (Figure on page 1003)
Internal hemorrhagic and cystic degeneration is the hallmark of SPT due to the fragile vascular network of the tumor. These imaging features are best appreciated at MR imaging (Fig 12).

Page 1005
Several features of lymphoma may help distinguish it from adenocarcinoma (31).

1. A bulky localized tumor in the pancreatic head without significant MPD dilatation. The MPD is typically mildly dilated in lymphoma but grossly dilated in adenocarcinoma. CBD dilatation is more common than MPD dilatation in lymphoma.

2. Enlarged lymph nodes below the level of the renal vein.

3. Invasive tumor growth that does not respect anatomic boundaries and that infiltrates retroperitoneal or upper abdominal organs and the gastrointestinal tract.

Page 1011 (Figure on page 1010)
IPAS has characteristics similar to those of the spleen at nonenhanced and contrast-enhanced imaging (Fig 21) (53).